


Temperature dependence of the band gap of $^{28}\text{Si}:\text{P}$ at very low temperatures measured via time-resolved optical spectroscopy

E. Sauter,¹ N. V. Abrosimov², J. Hübner^{1,*} and M. Oestreich^{1,†}

¹*Institut für Festkörperphysik, Leibniz Universität Hannover, Appelstraße 2, 30167 Hannover, Germany*

²*Leibniz-Institut für Kristallzüchtung, Max-Born-Straße 2, 12489 Berlin, Germany*

 (Received 5 August 2022; revised 3 February 2023; accepted 16 February 2023; published 15 March 2023)

We measure the temperature dependence of the indirect band gap of isotopically purified $^{28}\text{Si}:\text{P}$ in the regime from 0.1 K to 3 K by high-resolution absorption spectroscopy of the donor bound exciton transition. The measurements increase the up-to-date precision of the temperature-dependent band gap change by more than one order of magnitude and reveal a T^4 dependence which is about a factor of two less than observed in previous measurements. Such a T^4 dependence is predicted by theory, but the absolute values differ between our experiment and the most up-to-date calculations by a factor of 30, corroborating that the electron-phonon interaction at low temperatures is still not correctly included into theory. What is more, the ability of such very high-precision band-gap measurements facilitates the use of time- and spatially resolved $^{28}\text{Si}:\text{P}$ absorption as a contactless, local thermometer and electric field sensor with a demonstrated time resolution of milliseconds.

DOI: [10.1103/PhysRevResearch.5.013182](https://doi.org/10.1103/PhysRevResearch.5.013182)

I. INTRODUCTION

Phosphorous donors in silicon are auspicious candidates for efficient quantum computing, quantum communication, and radically new quantum technologies [1–5]. One game-changing ingredient for this rapidly advancing development is isotopically purified ^{28}Si , which has zero nuclear spin [6]. The material allows for the implementation of high-fidelity single qubits, electronically tunable qubit gates [7–10], and, since recently, even precision tomography of a three-qubit phosphorous donor quantum processor with an impressive two-qubit average gate fidelity of 99.37(11)% [11]. Furthermore, the doping of phosphorus ^{28}Si allows manipulation not only by electrical means but also optically. Thewalt *et al.* demonstrated in several landmark publications the efficient manipulation of the phosphorus donor-electron and nuclear spin using the optically active bound exciton transition in $^{28}\text{Si}:\text{P}$ [3–5,12]. Here, we improved the frequency stability of the resonant laser source by roughly an order of magnitude via stabilizing it to an ultra-low-expansion (ULE) cavity and tremendously reduced the environmental hydrostatic pressure onto the silicon sample compared to the previous measurements, which in turn reduces the influence of temperature-dependent pressure shifts. The donor bound exciton transitions in ^{28}Si typically have a full width at half-maximum of some tens of MHz [13] and are currently the narrowest optical transitions of ensembles of bound excitons

in any doped semiconductor. To date, the transitions of the exciton ensemble of the state-of-the-art $^{28}\text{Si}:\text{P}$ are still inhomogeneously broadened [14]. However, reaching the limit of homogeneous broadening seems feasible in the near future, promising very efficient coupling of electrical and optical quantum information processing [14].

The optical transition frequency of the phosphorus donor bound exciton (D^0X) is directly related to the indirect band gap of the Si host crystal via the bound electron ionization and exciton binding and energy, respectively, and its temperature dependence [15]. The absolute value of the zero-phonon line of the donor-bound exciton transition frequency at the lowest temperatures (0.7 K) in our experiments is 278.0332(1) THz, whereas the band gap of Si corresponds roughly to 282.905 THz [16] at $T < 4$ K. While there is a relative shift of the bound-exciton frequency in Si due to the temperature dependence of dielectric constant and effective masses, the ratio of these shifts in relation to the band gap temperature shift are on the order of only 2%, which is negligible for the purpose of the presented measurements [17].

As a consequence, the D^0X frequency can be rapidly adjusted locally for efficient optical addressing of subensembles of potential $^{28}\text{Si}:\text{P}$ qubits by imprinting a spatially and/or temporally varying temperature. Vice versa, the D^0X frequency can also be used as a contactless, all optical, local temperature sensor with high temporal resolution in $^{28}\text{Si}:\text{P}$ quantum devices. What is more, the temperature dependence of the D^0X transition at low lattice temperatures is not only interesting in view of $^{28}\text{Si}:\text{P}$ quantum devices but also from a fundamental point of view as a measure for the temperature dependence of the Si band gap. Cardona *et al.* measured between 1.3 K and 4.8 K in first approximation a T^4 dependence of the band-gap energy [17], which results, according to theory, from the total phonon energy in the Debye model for $T \rightarrow 0$. The derivation of this dependence on T^4 is straightforward, but the

*jhuebner@nano.uni-hannover.de

†oest@nano.uni-hannover.de

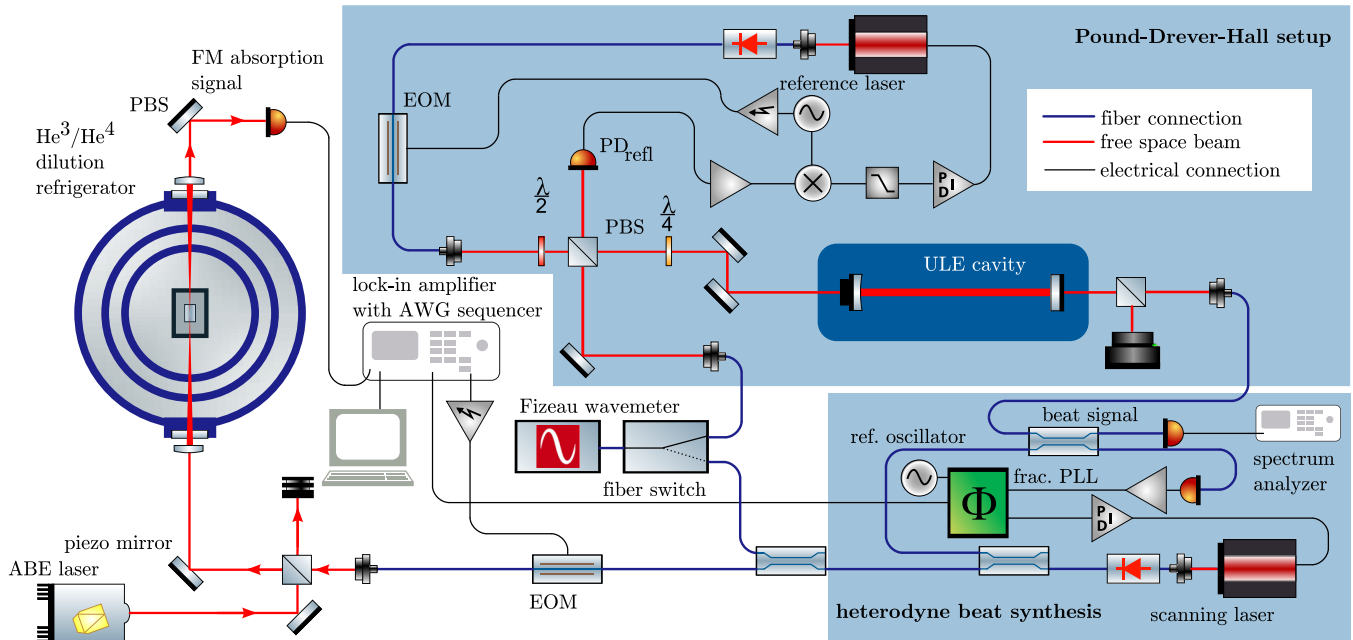


FIG. 1. Experimental setup. A cw reference laser (upper right) is frequency stabilized to an ULE cavity by Pound-Drever-Hall yielding a short- and long-term frequency stability of $\ll 100$ kHz. A second laser (lower right) used for frequency scanning is mixed with the reference laser, producing a beat signal. The frequency of this beat signal is stabilized to an electrical oscillator by a fractional phase-locked loop (PLL) which dictates the frequency offset of the scanning laser relative to the reference laser. A Fizeau wavemeter with 2 MHz accuracy is used for the initial approximate adjustment of the reference and scanning laser frequencies and for an independent continuous control of the laser frequencies. An electro-optic modulator (EOM) rapidly modulates the frequency of the scanning laser for FM absorption spectroscopy whereat a 600 MHz lock-in amplifier controls the fractional PLL reference oscillator and demodulates the FM absorption signal detected by a photo diode. A third laser for above band-gap excitation (lower left) is used for the time-resolved heating and cooling experiments only. Not shown are the lasers used for the positional control of the scanning laser beam in respect to the sample position. The lasers are isolated with fiber-coupled Faraday isolators and split via fiber Mach-Zehnder couplers.

calculations of its quantitative strength are excessively complex. Recently, Allen and Nery calculated the coefficient of the T^4 -dependent band gap using advanced computational techniques and found a discrepancy between theory and experiment by a factor of 60 [18]. The origin of this discrepancy is still unknown. On the one hand, the accuracy of the published measurement is restricted by the relatively large change of the pressure of the utilized liquid helium bath with temperature. This temperature-dependent He pressure alters the ^{28}Si band gap even more strongly than the actual investigated electron-phonon interaction [19] and yields over a certain temperature range also approximately a T^4 -dependent band-gap shift. On the other hand, the accuracy of the calculations is limited since the theory comprises electron-phonon coupling terms which cancel each other in first-order approximation such that the calculations easily might show some significant quantitative error.

II. EXPERIMENTAL SETUP

In the following, we experimentally study the temperature dependence of the D^0X transition in $^{28}\text{Si}:\text{P}$ by high-resolution absorption spectroscopy [20] in the temperature range from 0.1 K to 3 K. The $^{28}\text{Si}:\text{P}$ sample is placed inside a cryostat (Fig. 1) into a sample insert with a helium gas pressure of 1 bar at room temperature. The sample insert is in tight thermal contact with the cryostat cold plate via a solid rod of

oxide-free copper at which the temperature is measured via a calibrated RuO_2 sensor. The sample insert itself is machined out of beryllium-copper with a spherical bore inside which the sample is carefully laid down and loosely constrained by polytetrafluoroethylene elements in order to avoid larger movements during mounting the insert. The spherical bore is hermetically closed by two compressing rings and indium seals to which windows have been attached with epoxy glue. The closing procedure takes place within a glove box under ambient He pressure. In order to additionally rule out the significance of any thermal radiation heating, we performed sample temperature reference measurements with completely closed cryostat windows, leading to a decrease of the cold-plate temperature by only 30 mK, which is insignificant for all results presented here. The He pressure follows the van der Waals equation for temperatures above the dew point of ~ 1.4 K and is given by the T_{58} temperature scale [21] below the dew point. The temperatures of the helium gas and the sample are very close to the cold-plate temperature from which, in turn, the helium pressure is also calculated. The inset of Fig. 2 depicts the resulting temperature-dependent ^4He pressure, which depends approximately linearly on the temperature above the dew point and becomes negligible at ≤ 1 K. Exact knowledge of the pressure of the He gas is of great importance since the band gap depends not only on temperature but also on pressure [19]. Adequate cooling of the sample is determined around and above the dew point

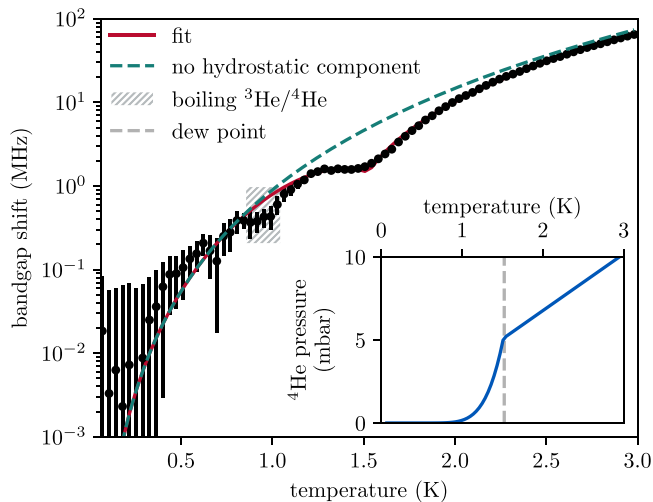


FIG. 2. Temperature dependence of the band gap of silicon measured via the no-phonon line of the D^0X transition. The insert shows the calculated pressure of the helium gas inside the sample container.

by efficient heat transfer by the ^4He gas and below the dew point by heat transfer of the ^4He superfluid phase. We want to point out that the highest gas pressure in our experiment is only ~ 10 hPa at 3 K, which is approximately two orders of magnitude lower than the maximal helium pressure in the first and only comparable publication, which measured the temperature dependence of the band gap using not the phosphorous donor but the boron acceptor exciton transition [17].

Figure 1 shows the experimental setup for our specially designed high-resolution, frequency modulated (FM) absorption spectroscopy experiment. One diode laser with a frequency close to the D^0X transition is locked as a stable reference by the Pound-Drever-Hall technique to a passive, ultra-low-expansion, optical cavity with an estimated drift of less than 0.1 Hz s^{-1} , which is negligibly small for the following experiments. A second external cavity diode laser is scanned mode-hop-free over a range of 400 MHz with a scanning velocity of 200 GHz s^{-1} . High-speed scanning with precise frequency control relative to the reference laser is achieved by mixing some fraction of the reference and scan lasers in order to generate a heterodyne beat signal. This beat signal is compared in a fractional phase-locked loop (Hittite HMC703) with an electronically synthesized, time-dependent frequency equal to the currently desired laser frequency difference. The resulting error signal of the phase-locked loop is used in combination with a fast Proportional-Integral-Differential-like laser controller to steer the optical frequency of the scanning laser. The remaining fraction of the stabilized scanning laser output is modulated with ~ 41 MHz by a fiber-based electro-optical phase modulator generating sidebands relative to the fundamental optical laser frequency. The modulation frequency matches roughly half the absorption width of the $^{28}\text{Si:P}$ transition and is precisely optimized to suppress any perturbing residual interference inside the optical fiber modulator.

The FM absorption measurements are performed by repetitively sweeping the optical center frequency of the scanning laser over the $^{28}\text{Si:P}$ exciton absorption peak. A piezo-actuated mirror is used to actively fix the position of the laser

beam to a well-defined sample volume in order to exclude any potential frequency changes by temperature-dependent changes of the sample position. This positional control is achieved by two additional lasers, which are pointing at sharp edges of the sample insert and give positional feedback without striking the sample. Temporal positional changes are additionally suppressed by regulating the still pressure of the cryostat with an accuracy of better than 1×10^{-3} bar in the temperature range from 0.05 K to 0.7 K. The focal spot of the scanning laser has a full width at half maximum at the sample of $\sim 190 \mu\text{m}$. The intensity of the scanning laser is kept constant at all times and all laser frequencies, and the absorption spectra acquired repeatedly at a given temperature are averaged in order to increase the signal-to-noise ratio. The maximum absorbed laser power at the D^0X absorption peak in the following experiment does not exceed the limit of $\sim 320 \text{ nW}$, at which several control experiments have excluded any significant heating of the sample, *inter alia* a time-dependent change of the D^0X frequency below only 200 kHz for the given probe laser power. The absorption coefficient is measured at a peak value of 0.14 m^{-1} . Losses due to multiple cryostat windows providing thermal insulation are estimated at 25% by a control measurement without sample. In addition, the reflectivity of the sample surface is estimated at 33%. The laser power is measured in front of the cryostat and the absorbed power is calculated accordingly. The measurements are carried out at zero external magnetic field such that optical pumping of electron and nuclear spins can be neglected. The inhomogeneous absorption linewidth is in this case for all temperatures $\lesssim 100$ MHz, which is not limited by the isotopic concentration of the $^{28}\text{Si:P}$ sample but dominated by the finite phosphorous doping concentration of $1.2 \times 10^{15} \text{ cm}^{-3}$. In principle, the donor bound exciton $^{28}\text{Si:P}$ absorption lines are narrower at a finite magnetic field and thereby better suited to measure frequency shifts of the band gap, but the extremely long electron spin relaxation times at temperatures below 1 K [22] make undisturbed measurements without relevant optical pumping more challenging at finite magnetic fields.

III. TEMPERATURE DEPENDENCE OF THE BAND GAP

The black dots in Fig. 2 show the measured absolute value of the D^0X frequency shift as a function of the cryostat temperature. The extracted average frequency deviations are about 200 kHz at all temperatures and are depicted as black vertical error bars. The goal of this experiment is to extract the exact functional dependence of the temperature dependence of the D^0X transition and accordingly of the ^{28}Si band gap at zero pressure. Therefore, we fit the measured frequency shift $\delta(T)$ by

$$\delta(T) = AT^p + k_h P(T), \quad (1)$$

where A is the sought-after coefficient of acoustic phonon coupling [18], the exponent p is expected to approach 4 for $T \rightarrow 0$ in the framework of the Debye model, k_h is the sample-specific coefficient of the hydrostatic pressure shift at rather low pressures, and $P(T)$ is the calculated pressure of the helium exchange gas depicted in the inset of Fig. 2. The red line in Fig. 2 shows a fit to the experimental data accord-

ing to Eq. 1 with $A = -0.90(5) \text{ MHz K}^{-p}$, $p = 4.03(5)$, and $k_h = 0.64(5) \text{ MHz hPa}^{-1}$. Most notably, the free fitting parameter p yields in this low-temperature regime with very high experimental accuracy the exponent of 4, as predicted by theory. Compared to the data in Ref. [17], the measurement accuracy is much higher, and even more important, the temperature dependence of the band-gap shift is not obscured by any pressure-dependent band-gap shift with a similar temperature dependence and significantly larger amplitude. In other words, our experiment has the advantage of much lower pressure changes, a linear pressure dependence for $T \geq 1.4 \text{ K}$, and a standardized gas pressure from the T_{58} temperature scale [21] for $T < 1.4 \text{ K}$.

A comparison of the dashed green line and the solid red line in Fig. 2 shows the influence of the He gas pressure in our experiment. Here, the dashed green line is calculated with the same fitting parameters as the solid red line but with k_h set to zero. The relative influence of the gas pressure is strongest in our case around the dew point at 1.4 K. At higher temperatures, the relative influence of the He gas pressure becomes smaller, since the phonon-dependent band-gap shift increases with T^4 but the gas pressure-induced shift increases only linearly with T . Well below the dew point, the relative influence also decreases, since the He pressure approaches zero in the limit of $T \rightarrow 0$. We want to point out that the experimental data in the dashed area around 0.9 K is affected by some small systematic errors due to the boiling of the $^3\text{He}/^4\text{He}$ mixture in the dilution cryostat, which introduces quick movements of the Si sample holder, which are too fast for the positional control. We also want to point out that the pressure coefficient k_h of Eq. 1 differs not only by amplitude but also by sign compared to the measurements at relatively high pressures in Ref. [17]. We expect that this difference arises, *inter alia*, from the native oxide layer of the Si sample, which introduces additional strain and changes the response of the band gap to small hydrostatic pressure (see the Appendix D for details).

Next, we discuss the acoustic phonon coupling coefficient A . Our measurements reveal an acoustic phonon coupling coefficient, which is about a factor of two smaller compared to the value extracted in Ref. [17]. We verified the value presented here by a modified secondary absorption measurement, which extends to higher temperatures for the sake of lower absolute precision. This secondary experiment confirms the discrepancy by a factor of about two such that we can exclude with high probability an experimental artifact in our experiment. One might think that different changes in the donor versus acceptor excitonic binding energy with temperature could be the reason for this difference, but the change in the excitonic binding energy versus the change in the band gap should be less than 2% and therefore negligible [17].

In total, a comparison of our high-precision experimental data on the acoustic phonon coupling coefficient with the most up-to-date theory yields a discrepancy between our experiment and theory by a factor of about 30, taking the theoretical estimate of $A = -0.3 \text{ MHz K}^{-4}$ [18]. The precision of our data excludes experimental details as a cause for this discrepancy and thereby spotlights the nontrivial difficulties in calculating the relevant electron-phonon interaction quantitatively. In fact, the significant overestimation of the electron-phonon

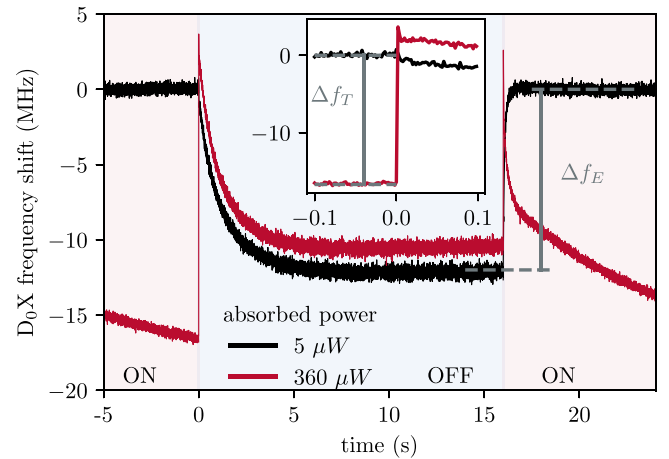


FIG. 3. Temporal shift of the D^0X resonance frequency for $5 \mu\text{W}$ (black line) and $360 \mu\text{W}$ (red line) ABE power, respectively. The ABE is periodically switched on and off periodically for 16 s whereat the moment of switching off defines $t = 0$. The complete dynamics results from changes of temperature, changes of the charge states of donors and acceptors, and long-living surface electric fields at which Δf_T is the frequency change due to the temperature change and Δf_E is the frequency change due to the change of the electric field induced by neutralizing the ionized donors and acceptors.

interaction by theory strongly suggests that the cancellation of the acoustic-phonon contributions is not completely included in the current calculations yet.

IV. TIME-DEPENDENT HEATING AND COOLING

In the following, we apply the above very precise measurements of the D^0X frequency shift with temperature and use this shift as a fast, local, contactless, all-optical temperature and electric field sensor. Such a fast temperature sensor is of practical relevance, as local heating significantly changes the properties of potential $^{28}\text{Si:P}$ qubits. In principle, the local temperature could also be measured contactlessly by measuring the stationary electron or nuclear spin polarization in a small magnetic field. However, the longitudinal spin relaxation times in very pure $^{28}\text{Si:P}$ are extremely long at low temperatures, preventing the practical use of these entities for time-resolved temperature measurements.

We use an additional laser for the following time-dependent heating and cooling experiment for above-band-gap excitation (ABE) in order to create free carriers which relax via optical and acoustic phonon emission and heat the sample locally. The ABE laser is periodically turned on and off, and the resulting time-dependent frequency change is measured with a time resolution of 2 ms. Figure 3 shows the frequency change on a long time scale for a base temperature of 0.7 K and an absorbed ABE power of $\sim 5 \mu\text{W}$ and $\sim 360 \mu\text{W}$, shown as black and red lines, respectively. The zero point of the frequency shift is set to the equilibrium D^0X transition frequency that is reached when the $5 \mu\text{W}$ ABE has been switched on for a long time, i.e., for 16 s. At the same ABE power, the photoneutralization process takes roughly 500 ms, which is determined by the amount of free carriers generated per second in relation to the total amount of ionized acceptor-

donor pairs. The ABE laser is switched off at time equal to zero, and the Si sample cools down on a millisecond timescale towards base temperature. This fast cooling is observed for an ABE power of $360 \mu\text{W}$ (red line in Fig. 3) as a sudden jump of the D^0X frequency to $\sim +3$ MHz. There is no jump for the low ABE power of $5 \mu\text{W}$ since heating of the sample is negligible in this case. The reason why the jump for $360 \mu\text{W}$ does not end directly at 0 MHz and why the two depicted ABE powers do not converge after switching off the ABE laser is discussed later. After the quasi instantaneous jump when switching off the $360 \mu\text{W}$ ABE at $t = 0$, both D^0X frequencies decrease on a timescale of seconds and reach a quasi steady state after ~ 5 s. The response time of this multiexponential decay is approximately equal for both ABE powers. The decay is not attributed to cooling of the sample, which would have the opposite sign, but to a change of the quasi-static electric field induced by charged donors and acceptors. The excitation of free electrons and holes by ABE neutralizes charged donors and acceptors. After switching the ABE off, electrons from neutral donors recombine with holes from neutral acceptors, yielding stochastically distributed, ionized donors and acceptors whose electric fields shift the D^0X transition [23–25] by $\Delta f_E = 12.1(2)$ MHz. The magnitude of Δf_E can be linked to the acceptor background concentration n_a by calculating the average electrical field $\bar{E} \approx \{15.0 \pm 3.3\} \text{ V cm}^{-1}$ evoked by the ionized donor-acceptor pairs acting as randomly distributed dipoles [26] together with the energy shift of the D^0X transition due to the Stark effect. Taking the known coefficient of the Stark shift $S_{\text{Stark}} = \{0.80(17)\} \text{ MHz cm V}^{-1}$ [27] yields $n_a = 4.6(1.0) \times 10^{13} \text{ cm}^{-3}$, which is matching very well the boron concentration of $\sim 5 \times 10^{13} / \text{cm}^3$ measured by photoluminescence methods [13]. The attribution of this permanent shift to donor-acceptor recombination is supported by the multiexponential decay and the measured timescale of seconds, which are both observed in donor-acceptor photoluminescence (PL) recombination in low-doped Si [28]. A corresponding shift of the PL due to a change of the electric field has not been observed in the PL measurements carried out by Dirksen *et al.* [28] since these PL measurements were made on natural Si and the shift is extremely small compared to the large PL linewidth of n -doped, natural Si [29]. The decay time observed in Fig. 3 is (a) on the order of seconds, since donors and acceptors are at such a low doping level in relation to the Bohr radii very far apart, and (b) multiexponential, since the distance between individual donors and acceptors varies stochastically. Steady-state neutralization of charged donors and acceptors by ABE has been implemented in other experiments for high-resolution spectroscopy on unintentionally doped ^{28}Si so far, but these are to the best of our knowledge the first time-resolved measurements of the D^0X frequency shift in ^{28}Si due to donor-acceptor recombination-induced electric field changes. Please note that such a recharging of the acceptors does not take place in the case of purely resonant excitation of the D^0X , which has been used to measure the temperature dependence of the band gap depicted in Fig. 2, since resonant excitation of the D^0X does not create free holes, which are able to invoke a recharging of the local field environment.

Next, we discuss the jump to approximately $+3$ MHz at $t = 0$ s when switching the $360 \mu\text{W}$ ABE power off.

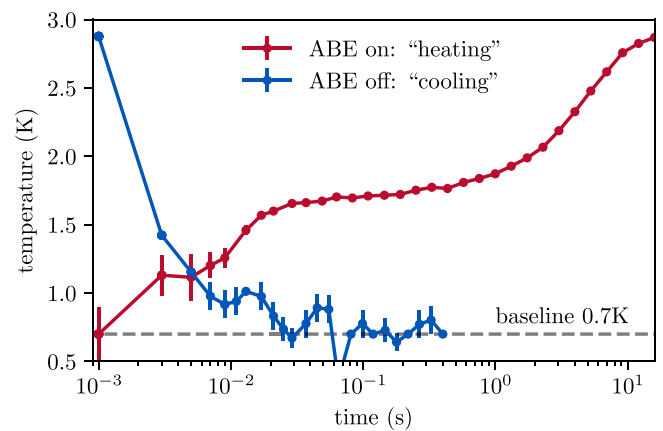


FIG. 4. Change of the lattice temperature with time for an absorbed ABE power of 0.6 mW and a base temperature of 0.7 K . The frequency change is converted to temperature according to Eq. 1 and the corresponding fitting parameters extracted from the data in Fig. 2.

Interestingly, the same jump to $+3$ MHz occurs when the $360 \mu\text{W}$ ABE power is switched on again (see the red line in Fig. 3 at $t = 16$ s). In both cases, donors and acceptors are fully neutralized and the sample is at the base temperature of 0.7 K . The almost instant neutralization of the impurities at $360 \mu\text{W}$ ABE power is corroborated by the rise time of less than 500 ms for an ABE power of $5 \mu\text{W}$ (see black line in Fig. 3 at $t \geq 16$ s), resulting in a calculated rise time of $< 7 \text{ ms}$ for $360 \mu\text{W}$. As a consequence, the shift to $+3$ MHz has to be attributed to the screening of another electric field, which has a decay time much longer than 16 s . The screening is significantly lower at $5 \mu\text{W}$, which is confirmed by the permanent 3 MHz shift between $360 \mu\text{W}$ and $5 \mu\text{W}$ while the ABE laser is still switched off for 16 s . The intensity dependence of the shift has been confirmed by several intensity-dependent control measurements (not shown). As a consequence, we attribute the shift to the screening of long-lasting surface electric fields as the only remaining possible source.

In another step, we study the copious heating and cooling dynamics which can be extracted from the measured frequency change because changes by the electric fields are easily identified and can be subtracted. The heating and cooling dynamics at higher ABE powers is obtained by subtracting the frequency change at lower powers since the time constant and amplitude of donor-acceptor reionization does not scale with higher powers. Another way to extract the temperature dynamics is to use ABE modulation periods much faster than the donor-acceptor recombination time. Figure 4 shows the extracted D^0X temperature shift due to ABE absorption for a base temperature of 0.7 K and an on/off switching time of 16 s . The time-dependent temperature change reveals a surprising difference between the cooling and heating of the sample. The warm-up process (ABE on) has components on short and long timescales, while the cool-down process has only a single fast component. The slow component can be explained by the thermal capacity of the helium gas, which is heated convectively by the sample during the warm-up process, while the rapid cooling after the ABE is switched off results from the efficient thermal contact between the sample and the sample insert via a superfluid helium film.

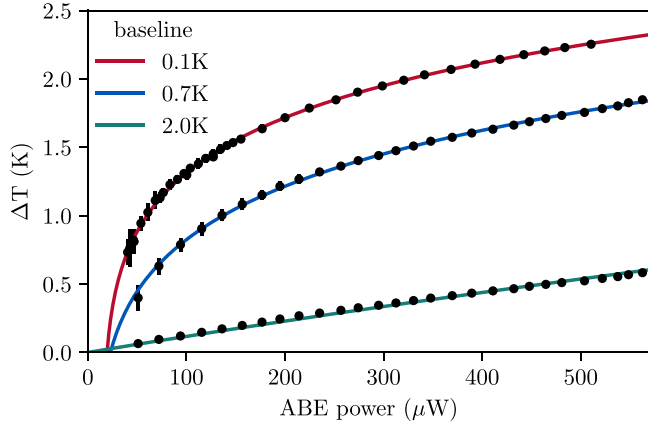


FIG. 5. Temperature change induced by above-band-gap excitation for different absorbed powers and base temperatures. The temperature change ΔT for base temperatures above the exchange gas dew point follows the behavior for gas-gap conductance in the Fourier limit. Lower base temperatures yield a heat transfer that scales approximately exponentially with ΔT .

The Rayleigh number of the helium exchange gas within our sample insert [30] is on the order of 10^4 , which supports thermal convection as the main heat transfer mechanism between the helium gas and the sample. Although the total absorbed power of the optical pulse is 8 mJ (under the same conditions as for the data shown in Fig. 4), an estimation of the energy required to heat the helium gas contained in the sample insert by 2 K yields a value of only 3.5 mJ. A lower heat absorption of the exchange gas is reasonable, because part of the power is transferred continuously to the sample insert during the heating process. The details of the heat transfer are further discussed in Appendix B.

Figure 4 shows that the cooling of the sample to base temperature is faster than 10 ms. As a consequence, fast on/off switching of the ABE with a period of 20 ms allows to measure the ABE-induced temperature difference of the sample, ΔT , with high accuracy. The fast periodic switching ensures in this process the quasi-steady-state neutralization of donors and acceptors and of the surface electric field, i.e., changes of the electric fields are negligibly small. Figure 5 shows the corresponding temperature differences ΔT measured in dependence on ABE power for three different base temperatures. For a base temperature below the dew point, the heat transfer scales in first approximation exponentially with ΔT (red and blue lines). Such an exponential increase of the heat transfer at low base temperatures indicates a significant contribution of ballistic helium atoms at which the helium density increases exponentially with temperature. For temperatures above the dew point, ΔT scales in first approximation linearly with the ABE power. This quasilinear dependence for relatively small temperature changes can be straightforwardly calculated as heat flow per contact area by nonballistic gas-gap conductance [31],

$$\dot{Q} = \frac{f k_B}{12 \sigma} \bar{v} \frac{\Delta T}{d} = \frac{f k_B}{12 \sigma} \sqrt{\frac{8k_B T}{\pi m}} \frac{\Delta T}{d}, \quad (2)$$

where $f = 3$ are the three translational degrees of freedom, \bar{v} is the average velocity, σ the effective atomic cross section,

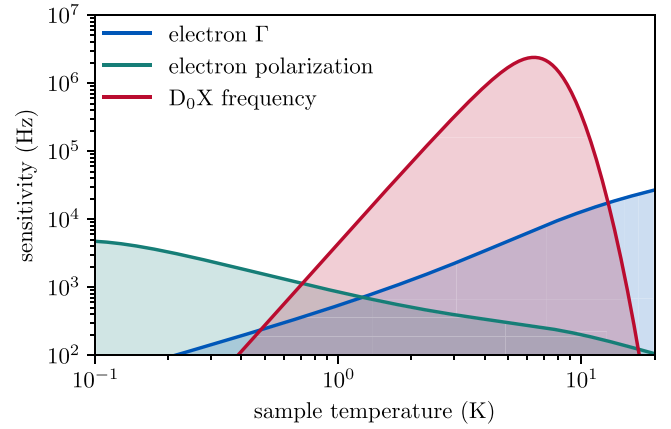


FIG. 6. Calculated relative sensitivity of contactless temperature measurements for three different physical principles.

m the mass of the helium atom, k_B the Boltzmann constant, and d the average gap distance between the sample and the copper underneath. Fitting Eq. (2) to the measured temperature change ΔT depicted in Fig. 2 for the base temperature of 2 K yields as the only free fitting parameter the average gap distance $d = 13.0(1) \mu\text{m}$, which is a reasonable value for the roughness of our milled and unpolished copper surface.

Last, we compare the performance of the $^{28}\text{Si}:\text{P}$ band-gap absorption as noncontact temperature sensor with nuclear and electron spin polarization as quantities for temperature measurements. Figure 6 shows the relative sensitivity for all three techniques in dependence on temperature. The calculations assume for the measurements of the electron or the nuclear spin polarization an external magnetic field of 0.1 T and a fixed uncertainty of the polarization measurement of 0.1% [32], and for the band-gap absorption measurements an accuracy of 0.2 MHz at low temperatures, which declines rapidly above 7 K because the width of the D^0X absorption peak increases in this regime due to phonon Raman scattering with T^7 . The calculations clearly show the excellent performance of such a band-gap absorption thermometer in the temperature range from about 1 K to 10 K. We want to point out that the measurement rate of the band-gap absorption thermometer is, in principle, limited only by the extremely fast phonon thermalization time, while a spin polarization thermometer is limited by the extremely long spin relaxation time at low temperatures. The electron spin relaxation time in $^{28}\text{Si}:\text{P}$ reaches, for instance, approximately 16 h at a sample temperature of 0.5 K and a magnetic field of 60 mT [22], making practical applications as a time-resolving thermometer very difficult.

V. CONCLUSION

Low-temperature, high-resolution absorption measurements attest a temperature dependence of the indirect band gap of ^{28}Si which is, with a very high experimental accuracy, proportional to T^4 . This dependence on T^4 agrees perfectly with the prediction of the Debye model in the limit of $T \rightarrow 0$. However, the associated acoustic phonon coupling coefficient, which has been ratified from our side by control experiments, is about two times smaller compared to the only other

existing experimental data and about a factor of 30 smaller than state-of-the-art predictions from theory. Such a strong discrepancy between experiment and theory seems surprising, but it underlines the theoretical challenge to include electron-phonon coupling and its canceling terms of opposite signs on a quantitative level. We expect that this challenge is not limited to ^{28}Si but exists for any nonpiezoelectric semiconductor.

The experimental data also reveal at very low pressures an unusual shift of the D_0X transition with hydrostatic pressure. This shift has the opposite sign in comparison to well-established hydrostatic energy shifts in bulk Si at high pressures, and probably results from additional strain due to natural oxidation of the silicon surface. This hypothesis is corroborated by a control experiment in which the native oxide was removed. Such subtle changes are generally not observable and are not relevant in natural silicon, but they play an important role for replicable D_0X transitions in view of optical manipulation of phosphorous donor quantum bits in $^{28}\text{Si:P}$.

The resulting detailed knowledge of the temperature and pressure dependence allows us not only to specifically adjust the optical transition frequency of the ^{28}Si qubits but also to use this transition as a fast and contactless temperature and electric field sensor. The switching of the qubit transition by temperature is demonstrated on a millisecond timescale at which the prospective limit of the switching frequency should be given by the very fast phonon dynamics and be in the GHz regime. The use of the D_0X transition as a temperature and electric field sensor yields the complex cooling and heating dynamics of strain-free mounted ^{28}Si systems and subtle changes of intrinsic stochastic electric fields via donor-acceptor recombination. The measured dynamics of this stochastic electric field takes place on a much longer timescale than the temperature change and shows a dynamic shift of the qubit transition by 12.1(2) MHz. Such stochastic internal electric fields are generally detrimental to qubit operations, but the identification of the physical origin allows for effective countermeasures. Interestingly, the measured shift is on the same scale as the hole-burning linewidth measured by Yang *et al.* in ^{28}Si [14], i.e., our experiment also suggests a course of action towards lifetime-limited hole burning in ^{28}Si . Such a kind of hole burning is exciting for quantum information processing, since homogeneously broadened ensembles of donors cannot be fabricated so far despite intensive, in-depth material development and research.

In summary, the presented research yields (a) by far the most precise measurement of the temperature dependence of the ^{28}Si band gap, that is, of any semiconductor; (b) a fundamental challenge of its theoretical description; (c) fast switching of the qubit transition by temperature; (d) a fast temperature and electric field sensor; (e) a detrimental stochastic electric field dynamics due to donor-acceptor recombination; and—by identification of this disruptive mechanism—(f) a likely solution towards homogeneously broadened ensemble transitions in ^{28}Si .

ACKNOWLEDGMENTS

This work was funded by the Deutsche Forschungsgemeinschaft (DFG, German Research Foundation) under Ger-

many's Excellence Strategy - EXC-2123 QuantumFrontiers - 390837967, Research Training Group 1991, OE-177/10-2, and OE-177/12-1.

APPENDIX A: METHODS

1. Sample and cryogenics

The sample (Si28-10Pr10.6.1PeFz3.1.6) consists of ultra-pure bulk ^{28}Si from the Avogadro project with an isotopic purity of 99.995% and a very low background impurity concentration, which has been *n*-doped with a nominal phosphorus doping concentration of $n_d = 1.2 \times 10^{15} \text{ cm}^{-3}$ and cut and polished to a size of $4 \times 2 \times 0.8 \text{ mm}$. The sample is placed strain-free in a specifically designed, vacuum-sealed, helium gas sample chamber coupled to the cold finger of a cryogen-free dilution refrigerator (Oxford Triton 400).

2. Spectroscopy

The scanning external cavity diode laser frequency offset is controlled relative to a cavity-stabilized reference laser using an optical phase-locked loop setup. The frequency stability of the system is estimated to be roughly 4 kHz. The scanning laser is phase modulated at 41 MHz and swept symmetrically with a speed of 400 GHz s^{-1} around the low-frequency peak of D^0X zero-field absorption spectrum (Fig. 7) multiple times to obtain an averaged low-noise spectrum. The low-noise master spectrum is obtained by averaging *all* acquired absorption spectra measured between 0.1 K and 1 K, where the shift in the absorption spectra is significantly smaller than the absorption linewidth. This master spectrum is used to fit the averaged spectra measured at a single temperature, at which the center frequency is the only fitting parameter. We assured that there is no significant alteration of the spectral shape by confirming the same standard deviation of difference spectra at the optimal shift value for the whole range of ABE powers and temperatures. This procedure yields extremely reliable results and an excellent signal-to-noise ratio. The zero-field absorption spectrum is described in great detail in Ref. [33]. In order to make sure that the relative stabilization of the

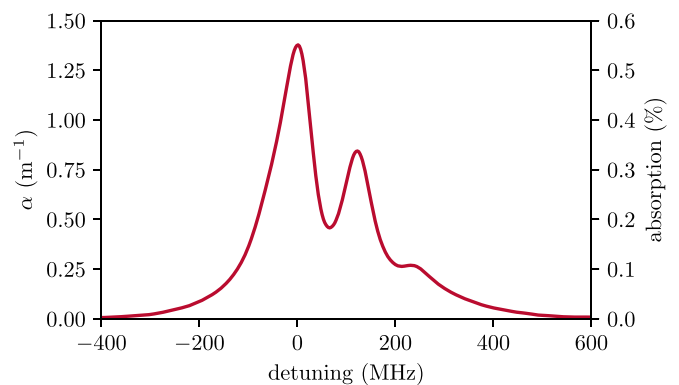


FIG. 7. Zero-field absorption spectrum of the donor-bound excitation transition. The low-frequency peak has a maximum absorption coefficient of $\alpha = 1.4 \text{ m}^{-1}$. The axis on the right shows the relative amount of light absorbed resonantly in our sample. The laser is scanned around the lowest frequency slope to obtain the highest PM absorption signal for measuring the frequency shift.

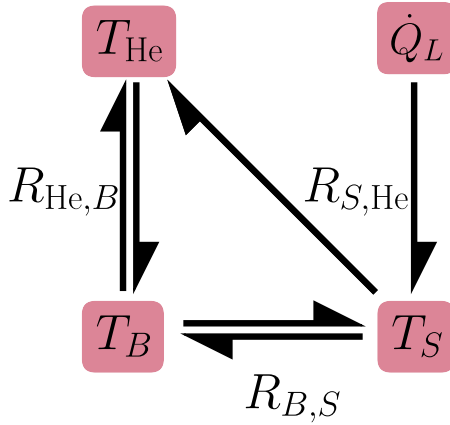


FIG. 8. Model for heat transfer within the sample insert. The laser is heating the sample (T_S) with a constant heat flow equal to the absorbed power \dot{Q}_L . The base temperature T_B is regulated via a temperature controller and assumed to be constant. The helium temperature is given by T_{He} . The corresponding differential equations are represented by Eqs. (B1)–(B3).

laser frequencies yields an accurate frequency control over the scanning range, the beat note between the reference and scanning lasers is detected via a spectrum analyzer to assure the relative frequency accuracy is within 4 kHz. From the error signal of the Pound-Drever-Hall feedback loop, we can also estimate the reference laser linewidth to be within a range of 4 kHz precision.

Straightforward calculations confirm that this evaluation method does not introduce any relevant variations to the extracted center frequency. The absolute resolution for detecting the D^0X frequency shift is estimated at 0.2 MHz. The ABE excitation source is set to emit at a wavelength of roughly 1022 nm. The scanning laser frequency is close to the donor-bound exciton transition. The reference laser frequency is tuned by roughly 2 GHz to the red with respect to the scanning laser and therefore detuned far enough from any resonant absorption. The spatial x and y positional lasers are derived from the reference laser source and both have a power of $1.2 \mu\text{W}$.

APPENDIX B: DIFFERENTIAL EQUATIONS FOR THE ABE INDUCED TEMPERATURE CHANGE

The red line in Fig. 4 shows that several distinct processes are involved in the heating of the sample, indicating that the dynamics of heat transfer within our system is not trivial. This section aims to provide an unpretentious and quantitative description of the underlying heating and cooling processes, neglecting the subtleties introduced by the superfluid He film at temperatures below 1.5 K. The basic model is schematically depicted in Fig. 8. The Si sample has a temporally variable temperature T_S and a thermal capacity C_S , which is according to the Debye model $\propto T^3$ in the low temperature limit studied. The helium gas has a temporally varying temperature T_H and a constant thermal capacity C_H of an ideal gas. The sample chamber is kept at a fixed temperature T_B and has in good approximation an infinite thermal capacity. The heat transfer is proportional to the respective temperature differences. Since

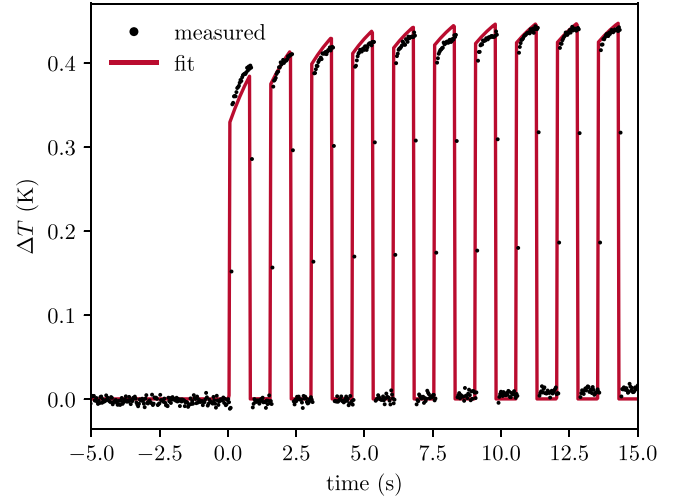


FIG. 9. Temperature response of the ^{28}Si sample for a pulsed ABE modulation with $360 \mu\text{W}$ absorbed ABE power, a base temperature of 2.0 K, and a modulation period of 1.25 s. The maximal sample temperature increases with each pulsed ABE because the helium exchange gas warms up. Then again, the sample temperature drops quickly to base temperature after each switching off of the ABE.

convection is the main mechanism for heat transfer between sample and helium gas, the thermal conductance between those two reservoirs acts only when the sample is warmer than the helium gas and is neglected in the opposite case. Given these assumptions, we arrive at a description of the heat flow given by the following set of equations:

$$\dot{T}_B = 0, \quad (\text{B1})$$

$$\dot{T}_S C_S = \frac{(T_B - T_S)}{R_{B,S}} + \frac{(T_{He} - T_S)}{R_{He,S}} \theta(T_S - T_{He}) + \dot{Q}_L, \quad (\text{B2})$$

$$\dot{T}_{He} C_{He} = \frac{(T_B - T_{He})}{R_{B,He}} + \frac{(T_S - T_{He})}{R_{He,S}} \theta(T_S - T_{He}), \quad (\text{B3})$$

where $R_{i,j}$ are constant thermal boundary resistances, θ is the Heaviside step function, and \dot{Q}_L is the heat power generated via ABE absorption.

We verify the model by an experiment in which the sample and the exchange gas are initially at base temperature, when at $t = 0$ a periodically pulsed ABE starts. The black dots in Fig. 9 show the resulting measured temperature change ΔT of the Si sample. The solid red line depicts a fit according to Eqs. (B1)–(B3) with the thermal boundary resistances as free parameters (see Table I). The comparison between measurement and fit clearly shows that the model is able to reproduce the three experimentally observed time regimes. One is very fast and corresponds to heat exchange between the interfaces of the ^{28}Si sample and the copper of the sample chamber, which are in rather close contact. The second one corresponds to heating of the helium exchange gas by the sample, while the third and slowest one corresponds to cooling of the total helium gas volume by the sample insert.

TABLE I. Parameters for the simulation of the measured heat flow shown in Fig. 9. The absolute thermal capacities are calculated from the mass of the sample and the density and volume of the helium gas. The thermal boundary resistances are extracted by fitting Eqs. (B1)–(B3) to the measured temperature response.

Boundary resistance		Thermal capacity	
	(mKW ⁻¹)		(mJ K ⁻¹)
$R_{\text{He},B}$	2.0(1)	C_S	$1.3 \times 10^{-8} \text{ K}^{-1-3} T_S^3$
$R_{S,\text{He}}$	1.0(3)	C_H	1.75
$R_{B,S}$	1.0(1)		

APPENDIX C: ELECTRICAL FIELD FROM RANDOMLY DISTRIBUTED DIPOLES

The average electrical field of the randomly distributed dipoles based on the ionized donor-acceptor pairs can be calculated according to Ref. [26]:

$$\bar{E} = \frac{\Gamma_{\text{dist}} d e_0}{4\pi\epsilon_0\epsilon_r r_0^3} \approx \{15.0 \pm 3.3\} \text{ V cm}^{-1}. \quad (\text{C1})$$

Here, $r_0 = (4\pi n_a/3)^{-1/3}$ is the approximated typical distance between the dipoles for an extracted acceptor density of $n_a = \{4.6(1.0) \times 10^{13}\} \text{ cm}^{-3}$, the dipole length d is approximated by the average donor distance $d = (4\pi n_d/3)^{-1/3}$ with $n_d = 1.2 \times 10^{15} \text{ cm}^{-3}$, e_0 is the unit charge, ϵ_0 and $\epsilon_r = 11.7$ are the vacuum and relative electrical permittivity, respectively, and $\Gamma_{\text{dist}} = \frac{\pi}{4} + \frac{\pi\sqrt{3}}{24} \text{arcsinh}(\sqrt{3})$ is an asymptotic approximation of the half width of the underlying Lorentzian field distribution.

APPENDIX D: STRAIN AND REMOVAL OF THE SILICON DIOXIDE LAYER

In order to confirm that the difference between the hydrostatic pressure coefficient from Fig. 2 compared to Ref. [17] is due to strain of the oxidized silicon surface, we removed the oxide by hydrofluoric acid and repeated the measurement.

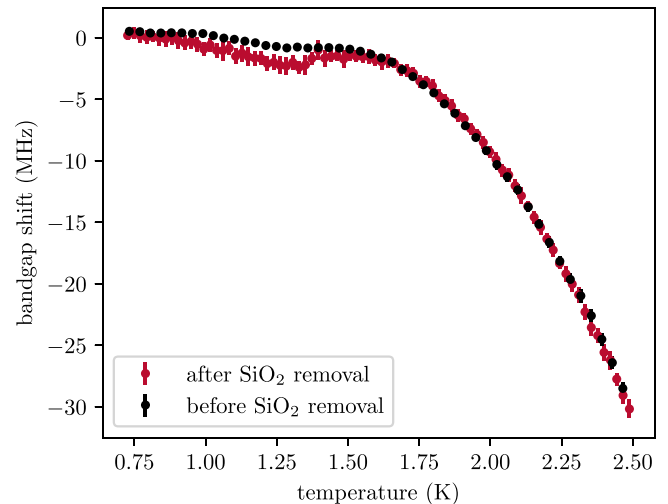


FIG. 10. Temperature dependence of the D_0X transition before and after removal of the natural silicon dioxide surface layer by etching the sample in hydrofluoric acid. The differences are most likely related to a change of the biaxial surface strain but other effects cannot unerringly be excluded.

Figure 10 shows, as expected, a significant change in the temperature dependence of the D_0X transition. Nevertheless, we want to point out that (a) the measured sample spot is not necessarily identical to the one before removal of the Si oxide, and that (b) although the sample insert is designed to avoid any strain but the hydrostatic strain evoked from the helium gas, we cannot perfectly rule out the existence of another source of strain acting on the sample that changed after reinstalling the sample insert. In both respects, further control experiments are necessary. Furthermore, the Si surfaces were not passivated and shortly exposed to air after the SiO_2 removal such that the surface morphology, strain, and Fermi level is unknown. In fact, the complex field of reproducible surface treatment will be an important issue if not *relative* changes of the D^0X transition frequency but reproducible *absolute* values are required for optical quantum information devices or metrology experiments.

[1] A. Morello, J. J. Pla, P. Bertet, and D. N. Jamieson, Donor spins in silicon for quantum technologies, *Adv. Quantum Technol.* **3**, 2000005 (2020).
 [2] M. J. Gullans and J. M. Taylor, Optical control of donor spin qubits in silicon, *Phys. Rev. B* **92**, 195411 (2015).
 [3] K. Saeedi, S. Simmons, J. Z. Salvail, P. Dluhy, H. Riemann, N. V. Abrosimov, P. Becker, H.-J. Pohl, J. J. L. Morton, and M. L. W. Thewalt, Room-temperature quantum bit storage exceeding 39 minutes using ionized donors in silicon-28, *Science* **342**, 830 (2013).
 [4] M. Steger, K. Saeedi, M. L. W. Thewalt, J. J. L. Morton, H. Riemann, N. V. Abrosimov, P. Becker, and H.-J. Pohl, Quantum information storage for over 180 s using donor spins in a silicon-28 “semiconductor vacuum,” *Science* **336**, 1280 (2012).
 [5] A. M. Tyryshkin, S. Tojo, J. J. L. Morton, H. Riemann, N. V. Abrosimov, P. Becker, H.-J. Pohl, T. Schenkel, M. L. W.

Thewalt, K. M. Itoh, and S. A. Lyon, Electron spin coherence exceeding seconds in high-purity silicon, *Nat. Mater.* **11**, 143 (2012).

[6] P. Becker, H.-J. Pohl, H. Riemann, and N. Abrosimov, Enrichment of silicon for a better kilogram, *Phys. Status Solidi A* **207**, 49 (2010).
 [7] Y. He, S. K. Gorman, D. Keith, L. Kranz, J. G. Keizer, and M. Y. Simmons, A two-qubit gate between phosphorus donor electrons in silicon, *Nature (London)* **571**, 371 (2019).
 [8] C. H. Yang, R. C. Leon, J. C. Hwang, A. Saraiva, T. Tantt, W. Huang, J. Camirand Lemyre, K. W. Chan, K. Y. Tan, F. E. Hudson, K. M. Itoh, A. Morello, M. Pioro-Ladrière, A. Laucht, and A. S. Dzurak, Operation of a silicon quantum processor unit cell above one kelvin, *Nature (London)* **580**, 350 (2020).
 [9] L. Petit, H. G. Eenink, M. Russ, W. I. Lawrie, N. W. Hendrickx, S. G. Philips, J. S. Clarke, L. M. Vandersypen, and M.

- Veldhorst, Universal quantum logic in hot silicon qubits, *Nature (London)* **580**, 355 (2020).
- [10] A. Morello, J. J. Pla, F. A. Zwanenburg, K. W. Chan, K. Y. Tan, H. Huebl, M. Möttönen, C. D. Nugroho, C. Yang, J. A. Van Donkelaar, A. D. Alves, D. N. Jamieson, C. C. Escott, L. C. Hollenberg, R. G. Clark, and A. S. Dzurak, Single-shot readout of an electron spin in silicon, *Nature (London)* **467**, 687 (2010).
- [11] M. T. Madzik, S. Asaad, A. Youssry, B. Joecker, K. M. Rudinger, E. Nielsen, K. C. Young, T. J. Proctor, A. D. Baczewski, A. Laucht, V. Schmitt, F. E. Hudson, K. M. Itoh, A. M. Jakob, B. C. Johnson, D. N. Jamieson, A. S. Dzurak, C. Ferrie, R. Blume-Kohout, and A. Morello, Precision tomography of a three-qubit donor quantum processor in silicon, *Nature (London)* **601**, 348 (2022).
- [12] A. Yang, M. Steger, T. Sekiguchi, M. L. W. Thewalt, T. D. Ladd, K. M. Itoh, H. Riemann, N. V. Abrosimov, P. Becker, and H. J. Pohl, Simultaneous Subsecond Hyperpolarization of the Nuclear and Electron Spins of Phosphorus in Silicon by Optical Pumping of Exciton Transitions, *Phys. Rev. Lett.* **102**, 257401 (2009).
- [13] M. L. W. Thewalt, A. Yang, M. Steger, D. Karaiskaj, M. Cardona, H. Riemann, N. V. Abrosimov, A. V. Gusev, A. D. Bulanov, I. D. Kovalev, A. K. Kaliteevskii, O. N. Godisov, P. Becker, H. J. Pohl, E. E. Haller, J. W. Ager, and K. M. Itoh, Direct observation of the donor nuclear spin in a near-gap bound exciton transition: ^{31}P in highly enriched ^{28}Si , *J. Appl. Phys.* **101**, 081724 (2007).
- [14] A. Yang, M. Steger, T. Sekiguchi, M. L. Thewalt, J. W. Ager, and E. E. Haller, Homogeneous linewidth of the ^{31}P bound exciton transition in silicon, *Appl. Phys. Lett.* **95**, 122113 (2009).
- [15] M. Cardona and R. K. Kremer, Temperature dependence of the electronic gaps of semiconductors, *Thin Solid Films* **571**, 680 (2014).
- [16] W. Bludau, A. Onton, and W. Heinke, Temperature dependence of the band gap of silicon, *J. Appl. Phys.* **45**, 1846 (1974).
- [17] M. Cardona, T. A. Meyer, and M. L. W. Thewalt, Temperature Dependence of the Energy Gap of Semiconductors in the Low-Temperature Limit, *Phys. Rev. Lett.* **92**, 196403 (2004).
- [18] P. B. Allen and J. P. Nery, Low-temperature semiconductor band-gap thermal shifts: T^4 shifts from ordinary acoustic and T^2 from piezoacoustic coupling, *Phys. Rev. B* **95**, 035211 (2017).
- [19] B. Welber, C. Kim, M. Cardona, and S. Rodriguez, Dependence of the indirect energy gap of silicon on hydrostatic pressure, *Solid State Commun.* **17**, 1021 (1975).
- [20] M. J. Thorpe, L. Rippe, T. M. Fortier, M. S. Kirchner, and T. Rosenband, Frequency stabilization to 6×10^{-16} via spectral-hole burning, *Nat. Photonics* **5**, 688 (2011).
- [21] H. A. Kierstead, Lambda curve of liquid He^4 , *Phys. Rev.* **162**, 153 (1967).
- [22] E. Sauter, N. V. Abrosimov, J. Hübner, and M. Oestreich, Low Temperature Relaxation of Donor Bound Electron Spins in $^{28}\text{Si} : \text{P}$, *Phys. Rev. Lett.* **126**, 137402 (2021).
- [23] A. M. Stoneham, Shapes of inhomogeneously broadened resonance lines in solids, *Rev. Mod. Phys.* **41**, 82 (1969).
- [24] J. Kato, K. M. Itoh, and E. E. Haller, Electric field broadening of arsenic donor states in strongly compensated n-type Ge:(As, Ga), *Phys. B: Condens. Matter* **302-303**, 1 (2001).
- [25] J. Kato, K. M. Itoh, and E. E. Haller, Observation of the random-to-correlated transition of the ionized-impurity distribution in compensated semiconductors, *Phys. Rev. B* **65**, 241201(R) (2002).
- [26] J. H. Wesenberg and K. Mølmer, Field Inside a Random Distribution of Parallel Dipoles, *Phys. Rev. Lett.* **93**, 143903 (2004).
- [27] C. C. Lo, M. Urdampilleta, P. Ross, M. F. Gonzalez-Zalba, J. Mansir, S. A. Lyon, M. L. W. Thewalt, and J. J. L. Morton, Hybrid optical-electrical detection of donor electron spins with bound excitons in silicon, *Nat. Mater.* **14**, 490 (2015).
- [28] P. Dirksen, A. Henstra, and W. T. Wenckebach, An electron spin echo study of donor-acceptor recombination, *J. Phys.: Condens. Matter* **1**, 7085 (1989).
- [29] R. C. Enck and A. Honig, Radiative spectra from shallow donor-acceptor electron transfer in silicon, *Phys. Rev.* **177**, 1182 (1969).
- [30] J. Niemela, Ultra-high Rayleigh number convection in cryogenic helium gas, *Phys. B: Condens. Matter* **284-288**, 61 (2000).
- [31] C. V. Madhusudana and C. Madhusudana, *Thermal Contact Conductance*, Mechanical Engineering, Vol. 79 (Springer, New York, 1996).
- [32] H. Marshak, Nuclear orientation thermometry, *J. Res. Na. Bur. Stand.* **88**, 175 (1983).
- [33] K. J. Morse, P. Dluhy, J. Huber, J. Z. Salvail, K. Saeedi, H. Riemann, N. V. Abrosimov, P. Becker, H.-J. Pohl, S. Simmons, and M. L. W. Thewalt, Zero-field optical magnetic resonance study of phosphorus donors in ^{28}Si , *Phys. Rev. B* **97**, 115205 (2018).